



1 **Population-wide Sampling of Retrotransposon Insertion**
2
3 **Polymorphisms Using Deep Sequencing and Efficient**
4
5 **Detection**

6
7
8
9
10
11 Qichao Yu^{1,2,†}, Wei Zhang^{1,2,†}, Xiaolong Zhang², Yongli Zeng², Yeming Wang², Yanhui Wang²,
12
13 Liqin Xu², Xiaoyun Huang², Nannan Li², Xinlan Zhou², Jie Lu³, Xiaosen Guo², Guibo Li^{2,4}, Yong
14
15 Hou^{2,4}, Shiping Liu^{2,5,*} and Bo Li^{2,6,*}

16
17
18
19
20
21
22 ¹ BGI Education Center, University of Chinese Academy of Sciences, Shenzhen 518083,
23
24
25 China

26
27 * Correspondence: libo@genomics.cn; liushiping@genomics.cn

28
29 † Equal contributors

30
31 Full list of author information is available at the end of the article.

32
33
34 14

35
36 15
37
38
39 **Emails of all authors:**

40
41 16 Qichao Yu: yuqichao@genomics.cn (ORCID: 0000-0003-2158-8424); Wei Zhang:

42
43 17 zhangwei7@genomics.cn (ORCID: 0000-0002-5792-7662); Xiaolong Zhang: 13528497060@163.com;

44
45 18 Yongli Zeng: zeoly100@163.com; Yeming Wang: 1398738509@qq.com (ORCID:

46
47 19 0000-0002-1521-2140); Yanhui Wang: 839584901@qq.com; Liqin Xu: xuliqin@genomics.cn; Nannan Li:

48
49 20 linannan@genomics.cn (ORCID: 0000-0003-3632-7964); Xinlan Zhou: zhouxinlan@genomics.cn

50
51 21 (ORCID: 0000-0001-9293-0894); Xiaoyun Huang: huangxiaoyun@genomics.cn (ORCID:

52
53
54
55
56
57
58
59
60
61
62
63
64
65

1 23 0000-0002-3389-9759); Jie Lu: lujie1@genomics.cn (ORCID: 0000-0001-7304-2023); Xiaosen Guo:
2 24 guoxs@genomics.cn (ORCID: 0000-0003-1317-2760); Guibo Li: liguibo@genomics.cn (ORCID:
3 25 0000-0002-6141-4931); Yong Hou: houyong@genomics.cn (ORCID: 0000-0002-0420-0726); Bo Li:
4 26 libo@genomics.cn; Shiping Liu: liushiping@genomics.cn (ORCID: 0000-0003-0019-619X).
5
6
7
8
9
10
11
12
13
14
15
16
17
18
19
20
21
22
23
24
25
26
27
28
29
30
31
32
33
34
35
36
37
38
39
40
41
42
43
44
45
46
47
48
49
50
51
52
53
54
55
56
57
58
59
60
61
62
63
64
65

Abstract

Background: Active retrotransposons play important roles during evolution and continue to shape our genomes today, especially in genetic polymorphisms underlying a diverse set of diseases. However, studies of human retrotransposon insertion polymorphisms (RIPs) based on whole-genome deep sequencing at the population level have not been sufficiently undertaken, despite the obvious need for a thorough characterization of RIPs in the general population.

Findings: Herein, we present a novel and efficient computational tool named Specific Insertions Detector (SID) for the detection of non-reference RIPs. We demonstrate that SID is suitable for high depth whole-genome sequencing (WGS) data using paired-end reads obtained from simulated and real datasets. We construct a comprehensive RIP database using a large population of 90 Han Chinese individuals with a mean 68 \times depth per individual. In total, we identify 9342 recent RIPs, and 8433 of these RIPs are novel compared with dbRIP, including 5826 Alu, 2169 long interspersed nuclear element 1 (L1), 383 SVA, and 55 long terminal repeats (LTR). Among the 9342 RIPs, 4828 were located in gene regions and five were located in protein-coding regions. We demonstrate that RIPs can, in principle, be an informative resource to perform population evolution and phylogenetic analyses. Taking the demographic effects into account, we identify a weak negative selection on SVA and L1 but approximately neutral selection for Alu elements based on the frequency spectrum of RIPs.

Conclusions: SID is a powerful open-source program for the detection of non-reference RIPs. We built a non-reference RIP dataset that greatly enhanced the diversity of RIPs detected in the general population and should be invaluable to researchers interested in many aspects of

50 human evolution, genetics, and disease. As a proof-of-concept, we demonstrate that the RIPS
51 can be used as biomarkers in a similar way as single nucleotide polymorphisms (SNPs).

52 **Keywords:** Transposable element, retrotransposon insertion polymorphism, next-generation
53 sequencing, whole-genome sequencing

54

55

56 **Findings**

57 **Introduction**

58 Transposable elements (TEs) are genomic sequences that can replicate within the genome
59 either autonomously or in conjunction with other TEs, resulting in insertion polymorphisms.
60 Over the evolutionary timescale, this process leads to drastic changes in genomic structure.
61 Current estimates suggest that approximately half of the human genome is derived from TEs
62 [1]. Retrotransposons, which constitute ~93% of TEs [2], can be subdivided into those
63 sequences containing LTRs and those that do not (non-LTR). The majority of human TEs
64 result from the activity of non-LTR retrotransposons, including the L1, Alu and SVA elements,
65 which collectively account for approximately one-third of the human genome [1]. Although
66 most retrotransposons are inactive remnants prevalent among the human population, younger
67 retrotransposons account for much of the structural variation among individual genomes [3].
68 Only a small proportion of total L1s are highly active [4]. The current rate of retrotransposition
69 in humans has been approximately estimated as 1 for every 20 births for Alu, 1 for every 200
70 births for L1 and 1 for every 900 births for SVA [5, 6].

71 Retrotransposon insertion is a disease-causing mechanism [7], and next-generation
72 sequencing (NGS) technology has been widely used to explore the association between
73 retrotransposon insertions and disease, such as cancer [8-10]. In this respect, a
74 comprehensive RIP dataset of a healthy population is necessary to serve as a reference for
75 the identification of disease-related RIPS. Based on the database of the 1000 Genomes
76 Project (1000GP), researchers performed RIP detection on an unprecedented scale and
77 detected thousands of novel RIPS [11-14]. This finding implies that an insertion allele present
78 in multiple individuals would effectively receive high coverage across the pooled dataset,

79 leading to a detection bias toward common insertions. It was previously estimated that at least
1 80 30x coverage of sequencing is needed to detect heterozygous RIPs with high sensitivity using
2 81 WGS [15].
3

4 82 Here, we developed the software SID to detect RIPs, which fulfilled our needs regarding
5 83 detection efficiency, accuracy and sensitivity. We also generated a non-reference TE insertion
6 84 polymorphism database by employing SID to analyze the whole-genome sequences of 90 Han
7 85 Chinese individuals (YH90) acquired at a mean depth of 68x.
8

9 86 **Materials and methods**
10

11 87 **Samples and whole genome sequencing**
12

13 88 We obtained B-lymphocyte cell lines from 90 Han Chinese individuals at the Coriell Institute
14 89 (Camden, New Jersey, USA). These individuals were selected from Beijing, Hunan province
15 90 and Fujian province, respectively. We broadly separated the samples into “Northern group” (45
16 91 samples) and “Southern group” (45 samples). DNA was extracted from the B-lymphocyte cells
17 92 of each individual, and libraries were then constructed following the manufacturer’s
18 93 instructions. High-coverage paired-end 100 bp WGS libraries were sequenced on the Illumina
19 94 HiSeq 2000 Platform. For more on this dataset see the Data Note describing its production
20 95 published alongside this paper [16]. In addition, we also used a Chinese sample [17] for which
21 96 the data were previously released in the European Nucleotide Archive (ENA) repository
22 97 (Additional file 1: Table S1). The Institutional Review Board on Bioethics and Biosafety of BGI
23 98 (BGI-IRB) approved the study.
24

25 99 **Processing of the WGS data**
26

27 100 Reads were aligned to the human genome reference (HG19, Build37) using *BWA* (*BWA* ,
28 101 RRID:SCR_010910)[18]. Duplications were removed using Picard tools, and the quality values
29 102 of each reads were recalibrated using the Genome Analysis Toolkit (GATK)(GATK ,
30 103 RRID:SCR_001876)[19]. The resulting Binary Alignment/Map (BAM) files were used as input
31 104 for SID (Additional file 2: Text S1).
32

33 105 **The specific insertion detector pipeline**
34

1 106 SID is compiled in Perl and includes the following two steps: discordant reads detection and
2 107 reads clustering. Generally, the first step collects informative reads and generates other
3 108 necessary files, whereas the second step discovers the specific insertion sites and exports the
4 109 final results into plain text.
5
6
7
8
9
10 110 *Detection of discordant reads.* The “discordant reads” were extracted for the subsequent
11 111 clustering step. Paired-end reads were determined as “discordant reads” if they met one of the
12 112 following criteria: a. one read mapped to HG19 uniquely and the other read mapped to the
13 113 retrotransposon library (multi-mapped or unmapped to HG19); b. one read mapped to HG19
14 114 uniquely and the other soft-clipped read mapped to HG19, and the clipped sequence could be
15 115 mapped to the retrotransposon library; c. one soft-clipped read mapped to HG19, and the
16 116 clipped sequence could be mapped to the retrotransposon library. The other read mapped to
17 117 the retrotransposon library (multi-mapped or unmapped to HG19). The retrotransposon library
18 118 includes objective TE classes, such as L1, Alu, and SVA. In this study, the TE reference
19 119 database contains known TE sequences collected from RepBase version 17.07 [20], dbRIP
20 120 [21] and Hot L1s [4]. To reduce the long processing time due to large volumes of WGS data,
21 121 we implemented a parallel approach to process each bam files of samples simultaneously in
22 122 the discordant reads detection step.
23
24
25 123 *Reads clustering and detection of breakpoints.* First, the “discordant reads” were scanned and
26 124 clustered into blocks that supported potential RIPs based on the Maximal Valid Clusters
27 125 algorithm [22]. Second, we extracted all reads located within the cluster regions and
28 126 determined the breakpoints. Although high-depth, data-enabled RIP detection with high
29 127 sensitivity was possible given that more soft-clipped reads neighboring target site duplication

1 128 (TSD) could be detected, alignments neighboring the TSDs had apparently lower depth
2
3 129 compared with the mean sequencing depth of the whole genome due to occasional
4
5 130 sequencing and system errors. This feature made breakpoint detection difficult and increased
6
7 131 the false discovery rate (FDR). Thus, we added the recalibration process of clipped points to
8
9 132 determine breakpoints. Each read located within the cluster regions flanking potential
10
11 133 breakpoints was used to confirm the precise location of the breakpoints. Small deletions were
12
13 134 extracted to perform breakpoint recalibration, and the mismatched bases were removed from
14
15 135 the deletion sequences.

21
22 136 The clipped sequences were realigned to local regions on HG19 to determine the actual
23
24 137 breakpoints. Breakpoints were assigned as “clips” if greater than half of the new clipped
25
26 138 sequences were discordant with the reference sequence and the length of gap within the new
27
28 139 clipped sequence was less than 30%. The point would not be a candidate unless it was a “clip”
29
30 140 and the mismatch was less than 5 bp or contained poly-A/T.

35
36 141 Some terminals of reads containing mismatched bases may be the clipped parts because
37
38 142 these bases were treated as mismatches rather than clips. The breakpoints candidates were
39
40 143 re-estimated by SID if mismatches accounted for greater than half of the read terminals.

44
45 144 Notably, we implemented the “Asynchronous Scanning” algorithm (Additional file 2: Text
46
47 145 S2). Using this algorithm, once the program clustered one possible insertion region by
48
49 146 scanning unique reads, the process of breakpoint detection in this region was immediately
50
51 147 performed, rendering it possible to detect TE insertions in one chromosome in only a few
52
53 148 minutes. The detailed algorithm for RIP candidate determination is provided in Additional file 2:
54
55 149 Text S2.

150 **Annotation of TE insertions**

1
2
3 151 *Orientation annotation for the TE insertions.* We annotated the orientation of TE insertions
4
5 152 based on the BLAST results [23]. First, we extracted the discordant repeat anchored mate
6
7 153 (RAM) reads and clipped reads that supported the TE insertion and made the reads'
8
9 154 orientations the same as HG19. Then, we realigned the supporting reads against the
10
11 155 consensus sequences of known active retrotransposons to identify the mapped orientation in
12
13 156 known active retrotransposons. The orientations of TE insertions were judged by the reads'
14
15 157 orientation (for details see Additional file 2: Text S3). The accuracy of orientation annotation
16
17 158 was assessed by comparing 396 matched insertions from dbRIP and 21 fully sequenced
18
19 159 insertions from PCR validation experiments (Additional file 1: Table S2). In total, 326 insertions
20
21 160 were verified, and the FDR of orientation annotation was 21.82%.

22
23
24
25
26
27
28 161 *Subfamily annotation for R IPs.* The subfamily annotation of R IPs was performed according to
29
30 162 known active retrotransposons. We first constructed a comprehensive retrotransposons
31
32 163 sequence library. Alu subfamily consensus sequences were acquired from RepBase 17.07
33
34 164 [20]. L1 subfamily consensus sequences were acquired from Eunjung Lee [10]. SVA and LTR
35
36 165 consensus sequences were acquired from Baillie [24]. Next, we performed multiple subfamily
37
38 166 sequence alignment for each type of retrotransposon and discovered the diagnostic nucleotide
39
40 167 for each subfamily (for details see Additional file 1: Table S3-5). Specially, we discovered the
41
42 168 diagnostic nucleotide of L1 from previous studies [25-28]. We then assembled the “discordant
43
44 169 reads” of each RIP into contigs using CAP3 [29] and realigned them against all of the
45
46 170 subfamily sequences using BLAST (NCBI BLAST , RRID:SCR_004870)[30] (Additional file 2:
47
48 171 Text S3-4).

1 172 *Length annotation for RIPs.* During mapping the contigs to subfamily sequences, we identified
2 173 the first mapped site of the 5' and 3' ends of the subfamily sequence and accordingly counted
3 174 the lengths from the initial site (L_{min} and L_{max}). The length of inserted retrotransposon (L_{retro})
4 175 was calculated as the difference between the maximum and the minimum length of the aligned
5 176 sequence, as follows:

$$L_{retro} = L_{max} - L_{min} + 1.$$

178 **Simulation of RIP data**

19 179 In total, 761 TEs were randomly selected from our reference TE database (see Materials and
20 180 methods: Annotation of TE insertions) and inserted into HG19 autosomes randomly to
21 181 generate a new human genome (for details see Additional file 1: Table S6). The pIRS [31]
22 182 software was used to generate approximately 60x paired-end 100 bp reads; then, we mapped
23 183 these reads to the HG19 genome by BWA. Then, we used SID to detect these RIPs in the
24 184 simulated genome. By repeating this process, we obtained results from simulated data with
25 185 different depths to assess the sensitivity and specificity of RIP detection in sequence data with
26 186 distinct depth using SID.

41 187 **Reference RIP detection**

44 188 The reference RIPs were detected as a subset of deletions of the samples relative to the HG19
45 189 reference (Additional file 2: Figure S1). These deletions were selected from the results of
46 190 structural variation (SV) detection of YH90 samples, and the RIPs were annotated based on
47 191 matched deletion coordinates to HG19 annotation of RepeatMasker (greater than 90% of them
48 192 overlap with each other) [32].

58 193 The reference RIPs should be absent in the chimpanzee genome. The alignments of

1 194 chimpanzee mapped to the human genome were downloaded from UCSC
2 195 (<http://hgdownload.cse.ucsc.edu>). One reference RIP candidate should correspond to a gap
3 196 with an overlap of greater than 90% to each other, and no gaps were present in the
4 197 chimpanzee genome at this locus. The RIP candidates were filtered if no polymorphisms were
5 198 present in the YH90 samples (i.e., the allele frequency was equal to 180).

14 199 **Results**

15 200 **Establishment of SID**

16 201 To detect non-reference RIPs from WGS data accurately and in a time-efficient manner, we
17 202 developed SID, which can detect non-reference RIPs easily and quickly through discordant
18 203 reads detection and reads clustering. In the first step, three types of informative discordant
19 204 reads were selected for further analysis (Fig. 1a). Then, the reads that had mismatched bases
20 205 at the terminals (Fig. 1b, 1c) were used for judging heterozygosity. The clipped reads were
21 206 used to confirm the sequence of TSD and the precise insertion site of certain TEs.

22 207 **Non-reference retrotransposon insertion calling**

23 208 To investigate the influence of sequencing depth on RIP detection sensitivity and accuracy, we
24 209 simulated sequence data at different depths. Detection sensitivity dramatically increased with
25 210 increasing sequencing depth and achieved 95% (730/761) when the sequencing depth was
26 211 greater than 30x. By contrast, detection accuracy slightly changed with increasing sequencing
27 212 depth (Fig. 2a).

28 213 We next estimated the RIP detection sensitivity using two real sequencing datasets. One
29 214 dataset was the CEU trio data, which was deep-sequenced (> 75x) Illumina HiSeq data
30 215 generated by the Broad Institute (father NA12891, mother NA12892 and the female offspring

1 216 NA12878) from the 1000GP. We first used SID to detect the RIPs of each individual in the CEU
2 217 dataset and evaluated the sensitivity by comparing the detection results with the
3 218 PCR-validated datasets from Stewart et al. [12]. For Alu, the mean sensitivity reached 96.3%
4 219 among individuals. We also obtained a mean sensitivity of 80.3% and 83.3% for L1 and SVA,
5 220 respectively (Additional file 1: Table S7).
6
7
8
9
10
11
12

13 221 The other dataset, including NA18571, NA18572 and NA18537, was also recruited in
14 222 1000GP. The RIP datasets of these three individuals detected by SID were larger and covered
15 223 70.08% of the same sample's results in 1000GP on average (Additional file 2: Figure S2). We
16 224 estimated RIP detection accuracy using the sequencing data from a lymphocytic cell line
17 225 (YH_CL, ~52x) obtained from an Asian individual. These data represent the first Asian diploid
18 226 genome dataset, and we performed PCR validation. We randomly selected 103 detected RIPs,
19 227 and 93/96 (7 loci were removed because of the poor primer specificity) loci were successfully
20 228 validated, indicating that SID had an accuracy of 90.29% - 96.88% (Additional file 1: Table S8
21 229 and Additional file 2: Figure S3 and Text S5). We also used the PCR validation result to access
22 230 the accuracy of genotyping, which was approximately 93.55% (87/93, Fig. 2b, Additional file 2:
23 231 Text S6).
24
25
26
27
28
29
30
31
32
33
34
35
36
37
38
39
40
41
42
43
44
45
46
47
48
49
50
51
52
53
54
55
56
57
58
59
60
61
62
63
64
65

232 We next compared the RIP detection efficiency of different methods (SID, RetroSeq [11]
233 and TEA [10]) using YH_CL and three samples (NA18571, NA18572 and NA18537) from
234 YH90 (Additional file 2: Text S7). The run time of SID was approximately 3-fold reduced
235 compared with the other two methods, suggesting that SID was the most time-saving method
236 among the three methods (Additional file 2: Table S9). SID and TEA had comparable
237 sensitivities that were increased compared with RetroSeq (Additional file 2: Figure S4). We

1 238 also validated the uniquely detected RIPs by PCR (Additional file 1: Table S10) with an
2 239 accuracy of 75.86% (22/29) and 77.78% (7/9) for Alu and L1, respectively, revealing a higher
3 240 RIP detection accuracy (Alu: 42.10% (8/19) and 82.61% (19/23) and L1: 66.67% (2/3) and
4 241 66.67% (2/3) for RetroSeq and TEA, respectively).

5
6
7
8
9 242 **A comprehensive RIP landscape of the Han Chinese population**

10
11
12
13
14 243 We then performed RIP detection on a much larger scale. We sequenced 90 Han Chinese
15
16 244 individuals and generated Illumina paired-end sequence data at an average depth of 68x for
17
18 245 each sample (Additional file 1: Table S1). Using SID, the high depth of the dataset (much more
19
20 246 than 30x) allowed us to build a comprehensive non-reference RIP landscape with high
21
22 247 confidence[16].

23
24
25 248 In total, we identified 9342 non-reference RIPs in autosome regions, including 6483 Alu
26
27 249 elements, 2398 L1s, 61 LTRs and 400 SVAs (Fig. 3a; for details, see Additional file 1: Table
28
29 250 S11 and Additional file 2: Text S8). Of this dataset, 8433 RIPs, including 5826 Alu elements,
30
31 251 2169 L1s, 383 SVAs, and 55 LTRs, were novel compared with dbRIP (Fig. 3b). The average
32
33 252 number of non-reference RIPs per individual was 1394 (ranging from 1304 to 1493, Fig. 3c),
34
35 253 including 1110.80 Alu elements, 231.34 L1s, 43.14 SVAs and 9.01 LTRs, and each type of RIP
36
37 254 had a similar proportion ($P = 0.6364$, $P = 0.2711$, $P = 0.2128$, $P = 0.5582$, respectively,
38
39 255 Wilcoxon signed-rank test). We compared pair-wise individuals of all 90 samples, and the
40
41 256 average specific loci number was 672.79, which is approximately half (48.25%) of
42
43 257 non-reference RIPs of one individual.

44
45
46 258 We next compared our results with the 1000GP SV dataset. In total, 34.94% (3264/9342)
47
48 259 of RIPs in YH90 were also found in the 1000GP dataset. The Pearson correlation coefficient

1 260 was 0.7998 ($P < 2.2 \times 10^{-16}$) between YH90 and all the 26 populations in 1000GP SV dataset.
2
3 261 The Pearson correlation coefficient was 0.8856 between YH90 and the East Asian (EAS)
4
5 262 population in 1000GP, which was higher than other populations ($r = 0.7662$, $r = 0.5741$, $r =$
6
7 263 0.7025 and $r = 0.7627$ for American (AMR), African (AFR), European (EUR) and South Asian
8
9 264 (SAS) populations, respectively. Additional file 2: Text S9)[14].
10
11
12 265 Specific insert location information enabled us to investigate genome-wide sequence
13
14 266 patterns of these non-reference RIPs. We observed that the non-reference RIPs varied among
15
16 267 chromosomes (Fig. 3d, e). Notably, we found that the two different subpopulations (from
17
18 268 southern and northern China) had similar patterns of RIP distribution ($r = 0.782$, Fig. 3e and for
19
20 269 details see Additional file 2: Figure S5). However, the distribution of non-reference RIPs was
21
22
23 270 not obviously correlated with GC content, fixed RIPs, or SNPs of the same sample within 10M
24
25 271 non-N bins (Additional file 2: Figure S6).
26
27
28 272 To further investigate the distribution of non-reference RIPs in the functional region, we
29
30 273 annotated all the inserted loci (Fig. 3f). Greater than half of RIPs (4828/9342) were located in
31
32 274 gene regions, and the majority of these were located in introns. Only 5/9342 RIPs were located
33
34 275 in protein-coding regions, including three genes, C1orf66 (Alu-inserted), SNX31 (Alu-inserted)
35
36 276 and APH1B (SVA-inserted), with low frequency (1/90) and two genes, ADORA3 (Alu-inserted)
37
38 277 and Slco1b3 (L1-inserted), with higher frequency (44/90 and 12/90, respectively). In addition to
39
40 278 gene regions, we also found that on average 9.78% and 4.93% RIPs were located in enhancer
41
42 279 regions and promoter regions per sample, respectively (Fig. 3f).
43
44
45 280 Furthermore, we annotated the subfamily, orientation and sequence length of all detected
46
47 281 inserted retrotransposons based on regional sequence assembly and remapping to the

1 282 retrotransposon library. The AluY sub-family constituted essentially all non-reference Alu
2 283 insertions, in which AluYa5 and AluYb8 were mostly active (Additional file 1: Table S11),
3 284 supporting conclusions from previous studies [26, 33, 34].
4
5
6
7
8
9 285 The orientation of one RIP is determined from the mapping orientation of contigs to a
10 286 retrotransposon reference and the existence of poly-A or poly-T tails of the inserted sequence
11
12 287 (Additional file 1: Table S11). Previous studies have reported that the gene-inserted RIP had a
13
14 288 greater influence on gene expression if it was inserted on the same orientation as the target
15
16 289 gene [2, 35]. However, we detected a comparable number of direct and reverse events (0.475
17
18 290 and 0.525, respectively), arguing against an obvious natural selection on the RIPS with
19
20
21 291 consistent orientation with the inserted gene.
22
23
24
25
26
27
28 292 Along with subfamily and orientation annotation, we also calculated the length of each
29
30 293 insertion sequence. We found that different types of TE insertions had different length
31
32 294 distributions (Additional file 2: Figure S7). Greater than half of Alu elements (~70%) were
33
34 295 full-length, whereas the length of the L1 was distributed more discretely. Most L1s (> 80%)
35
36 296 were fractured during the process of retrotransposon, which is consistent with a previous study
37
38 297 [13].
39
40
41
42
43
44 298 **RIPs of a healthy population**
45
46
47 299 The pure and comprehensive RIP dataset can be used as a baseline of healthy people for
48
49 300 other disease-related research, especially single-gene diseases. The candidate
50
51 301 disease-related retrotransposon insertions found in this dataset were filtered. We explicitly
52
53 302 measured the overlap between our dataset and the disease-related retrotransposon insertion
54
55
56 303 data in dbRIP (<http://dbrip.org>) [36]. None of the insertion sites existed in our dataset,

1 304 indicating the accuracy of the database. We also tested some cancer research data. We
2 305 tested the dataset of candidate cancer-related somatic retrotransposon insertions that was
3 306 strictly generated from data of The Cancer Genome Atlas (TCGA) Pan-Cancer Project for 11
4 307 tumor types. No overlapping RIPs were detected, whereas 43.36% germline retrotransposons
5 308 were detected. According to the comparison of colon cancer-specific data [9], we identified two
6 309 L1 insertions consistent with our dataset with frequency of 51/90 and 50/90. These two L1
7 310 insertions were germline retrotransposon insertions that were further validated by PCR
8 311 validation in Solyom's research. We also tested the candidate hepatocellular
9 312 carcinoma-specific insertions [8] and identified one L1 insertion that was also present in our
10 313 dataset with a frequency of 9/90. This site was finally validated as a germline insertion by PCR
11 314 in that research. In conclusion, our data provide a reference panel to exclude false positive
12 315 insertions related to cancer.

13 316 **Population evolution analysis**

14 317 To perform the population evolution analysis of RIPs, we first merged the non-reference RIP
15 318 dataset with the "reference" retrotransposon insertions that were polymorphic in YH90
16 319 samples (Additional file 2: Figure S1) to obtain all RIPs from our samples. The retrotransposon
17 320 insertions with a frequency equal to 1 were removed from our non-reference RIPs. The
18 321 "reference" RIPs were defined as the reference genome-specific retrotransposon insertions
19 322 compared with each individual of the YH90 group. These reference RIPs were selected from
20 323 the dataset of YH90 deletions, and only the RIPs absent in chimpanzee were retained.

21 324 Allele frequency spectrum (AFS) was not only influenced by the natural selection but also
22 325 by demographic history. For example, a low-frequency bias for the majority of mutations can

1 326 also be obtained if the population recently experienced a bottleneck [37].
2
3 327 To perform the neutral test more accurately, we took the demographic history into
4
5 328 consideration (Additional file 2: Text S10). We simulated the following two different
6
7 329 demographic scenarios: a two-epoch population with a recent contraction and a three-epoch
8
9 330 bottleneck-shaped history containing a reduction of effective population size in the past
10
11 331 followed by a recent phase of size recovery (Fig. 4a). We tested the different assumptions with
12
13 332 the SNP dataset (Fig. 4b and Additional file 2: Table S12), which supported that the
14
15 333 three-epoch model was the best model.
16
17 334 Next, we explored the possibility of using RIP information to perform population evolution
18
19 335 analysis. Based on the genotyping result of the merged RIP dataset, we described the RIP
20
21 336 AFS (Fig. 4c and Additional file 2: Text S11). The neutral model expectation can be calculated
22
23 337 using the formula θ/i , where θ is the insertion diversity parameter and i (180) is the allele
24
25 338 count in a fixed number of samples n (90) [37]. The spectrum was skewed toward low-allele
26
27 339 frequency compared with the distribution of the expected neutral model, indicating possible
28
29 340 negative selection pressure on retrotransposon insertions.
30
31
32
33
34
35
36
37
38
39
40
41
42 341 To investigate the influence of the demographic history on RIP AFS, we performed
43
44
45 342 demographic correction and re-analyzed the RIP AFS under different selection models (Fig. 4d
46
47
48 343 and Additional file 2: Figure S8-9). The classification of neutral with negative and positive
49
50 344 selection indicates that a proportion of RIPs was neutral, and a proportion of RIPs was under
51
52
53 345 negative selection. In addition, other RIPs were under positive selection (m1), neutral with
54
55
56 346 negative selection (m2), neutral with positive selection (m3), negative selection (m4), positive
57
58
59 347 selection (m5), and neutral selection (m6). We further calculated the selection coefficient (S')
60
61
62
63
64
65

1 348 under each best-fit model with the determination of an approximately neutral selection effect
2
3 349 threshold ($S' < 0.01\%$) [38]. Models m1 and m2 were the most fitted models with the observed
4
5 350 RIP AFS (Additional file 2: Table S13). The best-fit result of model m1 demonstrated that
6
7 351 approximately 75% RIPs were under negative selection with $s = 0.0290\%$, which indicates that
8
9 352 these RIPs are weakly deleterious. In addition, 10% were under positive selection, whereas 15%
10
11 353 were neutral. Under model m2, the best-fit result demonstrated that 70% of RIPs were under
12
13 354 negative selection with $s = 0.0396\%$. In addition, 30% of RIPs were neutral. The selection
14
15 355 coefficient was 0.0079% under the all negative selection model, indicating an approximately
16
17 356 neutral selection effect.

24
25 357 The distribution of fitness effects of retrotransposon subfamilies (L1, SVA and Alu) was
26
27 358 also estimated under the same demographic model. Assuming that all RIPs of different
28
29 359 subfamilies were under negative selection (model m1), the selection coefficient models were
30
31 360 various among three subfamilies of RIPs ($S' = -0.0143\%$, $S' = -0.0172\%$, $S' = -0.0068\%$ for L1,
32
33 361 SVA and Alu, respectively), suggesting that there is more natural selection pressure on L1 and
34
35 362 SVA (weakly negative selection) compared with Alu (nearly neutral selection).

41 363 **Phylogenetic analysis**

44 364 To investigate whether RIP information can be used to separate the Northern and Southern
45
46 365 Chinese groups, we performed principal component analysis (PCA) using the RIPs detected
47
48 366 from the YH90 dataset, which provided well-resolved Northern and Southern Chinese groups
49
50 367 (Fig. 5a and Additional file 2: Text S12). Compared with the PCA result derived from the SNPs
51
52 368 detected from the same dataset (Fig. 5b), there seemed to be more overlapping observations,
53
54 369 indicating SNPs might be more informative in resolving the two distinctive populations. Next,

1 370 we determined whether it is possible to perform phylogenetic analysis using RIP information
2 371 detected from the YH90 dataset. Two phylogenetic trees were constructed using RIPS and
3 372 SNPs, separately (Fig. 5c and 5d; for details, see Additional file 2: Text S13). Similar to the
4 373 PCA result, increased mixing between Northern and Southern Chinese individuals was
5 374 observed for the phylogenetic tree derived from the RIP information. Interestingly, HG00534,
6 375 an isolated Southern Chinese individual located in a northern cluster in the phylogenetic tree
7 376 established using the SNP information, clustered largely with Southern Chinese individuals in
8 377 the phylogenetic tree derived from the RIP information. Future studies are warranted to
9 378 explore whether combining SNPs with RIP results in the construction of a more accurate
10 379 phylogenetic tree.

11 380 **Conclusions**

12 381 In this paper, we developed the computer program SID to detect the non-reference RIPS of 90
13 382 healthy Han Chinese individuals using high-depth WGS. We described the landscape of RIP
14 383 distribution on population genomes and annotated the subfamily, orientation, and length of
15 384 RIPS. We demonstrated that the RIPS could be used as a normal baseline for
16 385 retrotransposon-related disease research.

17 386 To our knowledge, this is the largest Han Chinese genomics dataset to date. Compared
18 387 with 1000GP results from the same samples, approximately half (mean 48.05%; Additional file
19 388 2: Figure S2) of RIPS in our dataset were previously observed, suggesting that our
20 389 deep-sequenced data exhibited increased detection sensitivity compared with low coverage
21 390 data. For example, serum ACE levels were determined by the Alu insertion/deletion (I/D)

1 polymorphism in the following order: DD > ID > II [39]. The D allele of the ACE gene was
2 associated with essential hypertension in different populations [40-43]. We found that the ACE
3 gene harbored an Alu insertion in the 15th intron with a frequency of 81/90 in our 90 Chinese
4 genomes compared with a considerably reduced frequency (7/63) in CEPH individuals [12],
5 which was supported by a previous study [44]. To our surprise, no RIP ACEs were present in
6 Han Chinese samples from the 1000GP dataset, which is a high-frequency inserted gene in
7 our RIP data. ACE-specific PCR validation (Additional file 2: Figure S10) and a previous ACE
8 study [45] indicated that our results were consistent with the real values. This finding suggests
9 that adequate sequencing depth is important to investigate RIP frequency and that our data
10 present a result that is consistent with the actual situation. The highly sensitive and accurate
11 RIP dataset provided a perfect opportunity to perform RIP fitness analysis. This study
12 evaluates the natural selection effect on retrotransposon insertions at the population level. As
13 a type of long fragment insertion, RIPs are under approximately neutral selection. This finding
14 is consistent with our result that retrotransposon insertions are mostly relatively
15 inconsequential because the harbored genes are always relatively unimportant. Regarding
16 different types of RIPs in addition to Alu, the longer insertion elements L1 and SVA exhibit
17 weakly positive selection pressure.

18
19
20
21
22
23
24
25
26
27
28
29
30
31
32
33
34
35
36
37
38
39
40
41
42
43
44
45
46
47
48
49
50
51
52
53
54
55
56
57
58
59
60
61
62
63
64
65

408 This dataset can be compared with others to provide guidance in research of the
409 disease-causing mechanisms in certain populations and to successfully determine the
410 insertion time of a specific locus. This dataset can also be used as a standard for other RIP
411 research and can serve as a baseline to filter irrelevant RIPs in disease-causing
412 retrotransposon research. Genome-wide association studies (GWAS) have proven their utility

1 413 in identifying genomic variants associated with the risk for numerous diseases. Unlike SNPs
2
3 414 and copy number variations (CNVs) that are widely used in GWAS, RIPs have generally been
4
5 415 overlooked as a major contributor to human variation. Significantly, this dataset provides a
6
7 416 valuable resource to perform GWAS and identify more markers related to complex diseases.
8
9
10

11 417 The high cost of WGS at high depth is still a major limitation, preventing it from being
12
13 418 widely used in TE research. Furthermore, the large amount of data yielded by high-depth WGS
14
15 419 makes it difficult to undertake bioinformatic analysis. With the development of biotechnology
16
17 420 and IT, this situation should improve soon.
18
19
20
21

22 421 The next step is to research RIPs at the transcriptome level. The impact of RIPs on gene
23
24 422 expression remains unclear. Combining the genome and transcriptome would provide a
25
26 423 comprehensive picture about the regulation of RIPs. Thus, we can further expound the
27
28 424 position of the retrotransposon in the course of human evolution.
29
30
31 425
32
33
34 426 **Availability and requirements**
35
36
37

- 38 427 ● Project name: Specific Insertions Detector (SID)
39
40 428 ● Project home page: <https://github.com/Jonathanyu2014/SID>
41
42 429 ● Operating system(s): Linux
43
44 430 ● Programming language: Perl
45
46 431 ● Other requirements: Perl 5.14 or later, BLAST v2.2.25 or later, Samtools v1.0 or later
47
48 432 ● License: Apache License 2.0
49
50 433 ● Any restrictions to use by non-academics: None
51
52
53
54
55
56
57
58

59 434 **Additional files**
60
61
62
63
64
65

1 435 Additional file 1: Supplementary tables. Data description and the results of RIPs calling. (XLSX

2 436 1991 kb)

3 437 Additional file 2: Supplementary texts, figures and tables. (PDF 956 kb)

4 438 **Abbreviations**

5 439 CNV, copy number variation; ENA, European Nucleotide Archive; GWAS, genome-wide

6 440 association study; LTR, long terminal repeat; L1, long interspersed nuclear element 1; NGS,

7 441 next-generation sequencing; PCA, principal component analysis; RIP, retrotransposon

8 442 insertion polymorphism; SID, specific insertions detector; SNP, single nucleotide

9 443 polymorphism; TCGA, The Cancer Genome Atlas; TE, transposable element; TSD, target site

10 444 duplication; WGS, whole-genome sequencing.

11 445 **Acknowledgments**

12 446 We are grateful for Zengli Yan, Nan Li, Na Li and Runze Jiang for optimizing and testing the

13 447 SID program. We thank Haoxiang Lin and Wenjuan Zhu for providing technical assistance to

14 448 us. We thank Liang Wu and Xulian Shi for polishing the manuscript. We acknowledge the

15 449 support by the 1000 Genomes Project Consortium. This work was supported by the Shenzhen

16 450 Municipal Government of China [JSGG20140702161347218] and

17 451 [KQCX20150330171652450].

18 452 **Availability of data and materials**

19 453 The source code of SID is available from the GitHub and Zenodo repositories[46]. The human

20 454 (*Homo sapiens*) reference genome sequence (HG19) and its annotation files were

1 455 downloaded from UCSC Genome Bioinformatics (<http://genome.ucsc.edu/>). The raw
2 456 sequence data of YH_CL is available from the ENA repository (accession number ERA000005)
3
4 457 [47]. All the YH90 raw sequences have been released to the ENA repository (bioproject
5
6 458 number: PRJEB11005) and the processed data is also available from the *GigaScience*
7
8 459 GigaDB repository [48]. Snapshots of the code, alignments, and results files are also hosted in
9
10 460 GigaDB[49]. Protocols used for simulating reads for SNP Indel calling and detection of
11
12 461 transportable element insertions are also hosted in the protocols.io repository[50, 51].
13
14
15
16
17
18
19
20
21 462 **Authors' contributions**
22
23
24
25 463 BL, SL and YH initiated this project and reviewed the manuscript. QY, XZ, YZ and XH drafted
26
27 464 the manuscript. XH and JL edited the manuscript. QY, WZ, XZ and YW performed the data
28
29
30 465 analysis and drew the pictures. YZ and YW designed and developed the SID program. NL, XZ
31
32
33 466 and GL conducted the experiment for sequencing. LX designed the primers and performed
34
35
36 467 PCR validation. YH, BL, SL, XZ, XG and XH provided fruitful discussions.
37
38
39
40 468 **Competing interests**
41
42
43 469 The authors declare that they have no competing interests.
44
45
46
47 470 **Author details**
48
49
50 471 ¹ BGI Education Center, University of Chinese Academy of Sciences, Shenzhen 518083,
51
52
53 472 China. ² BGI-Shenzhen, Shenzhen 518083, China. ³ BGI College, Shenzhen 518083, China.
54
55
56
57
58
59
60
61
62
63
64
65

1 473 ⁴ Department of Biology, University of Copenhagen, Copenhagen 1599, Denmark.. ⁵ School of
2
3 474 Biology and Biological Engineering, South China University of Technology, Guangzhou
4
5
6 475 510641, China. ⁶ BGI-Forensics, Shenzhen 518083, China.
7
8
9
10 476 **Ethics, consent and permissions**
11
12
13 477 This study was approved by BGI-IRB (NO. 16101).
14
15
16
17 478 **Consent to publish**
18
19
20 479 Both BGI-IRB and participants involved consented to publish this research.
21
22
23 480
24
25
26
27 481 **References**
28
29
30 482 1. Lander ES, Linton LM, Birren B, Nusbaum C, Zody MC, Baldwin J, et al. Initial sequencing
31
32
33 483 and analysis of the human genome. *Nature*. 2001;409 6822:860-921.
34
35
36 484 2. Cordaux R and Batzer MA. The impact of retrotransposons on human genome evolution.
37
38
39 485 *Nature reviews Genetics*. 2009;10 10:691-703. doi:10.1038/nrg2640.
40
41
42 486 3. Kidd JM, Graves T, Newman TL, Fulton R, Hayden HS, Malig M, et al. A human genome
43
44
45 487 structural variation sequencing resource reveals insights into mutational mechanisms. *Cell*.
46
47
48 488 2010;143 5:837-47. doi:10.1016/j.cell.2010.10.027.
49
50
51 489 4. Brouha B, Schustak J, Badge RM, Lutz-Prigge S, Farley AH, Moran JV, et al. Hot L1s account
52
53
54 490 for the bulk of retrotransposition in the human population. *Proceedings of the National
55
56 491 Academy of Sciences of the United States of America*. 2003;100 9:5280-5.
57
58
59 492 doi:10.1073/pnas.0831042100.
60
61
62
63
64
65

- 1 493 5. Xing J, Zhang Y, Han K, Salem AH, Sen SK, Huff CD, et al. Mobile elements create structural
2 variation: analysis of a complete human genome. *Genome research*. 2009;19 9:1516-26.
3
4 494
5
6 495 doi:10.1101/gr.091827.109.
7
8 496 6. Cordaux R, Hedges DJ, Herke SW and Batzer MA. Estimating the retrotransposition rate of
9 human Alu elements. *Gene*. 2006;373:134-7. doi:10.1016/j.gene.2006.01.019.
10
11 497
12
13 498 7. Hancks DC and Kazazian HH, Jr. Active human retrotransposons: variation and disease. *Curr
14 Opin Genet Dev*. 2012;22 3:191-203. doi:10.1016/j.gde.2012.02.006.
15
16 499
17
18 500 8. Shukla R, Upton KR, Munoz-Lopez M, Gerhardt DJ, Fisher ME, Nguyen T, et al. Endogenous
19 retrotransposition activates oncogenic pathways in hepatocellular carcinoma. *Cell*. 2013;153
20
21 501
22
23 502 1:101-11. doi:10.1016/j.cell.2013.02.032.
24
25
26
27
28 503 9. Solyom S, Ewing AD, Rahmann EP, Doucet T, Nelson HH, Burns MB, et al. Extensive somatic
29 L1 retrotransposition in colorectal tumors. *Genome research*. 2012;22 12:2328-38.
30
31 504
32
33 505 doi:10.1101/gr.145235.112.
34
35
36 506 10. Lee E, Iskow R, Yang L, Gokcumen O, Haseley P, Luquette LJ, 3rd, et al. Landscape of somatic
37 retrotransposition in human cancers. *Science*. 2012;337 6097:967-71.
38
39 507
40
41 508 doi:10.1126/science.1222077.
42
43
44 509 11. Keane TM, Wong K and Adams DJ. RetroSeq: transposable element discovery from
45 next-generation sequencing data. *Bioinformatics*. 2013;29 3:389-90.
46
47 510
48
49 511 doi:10.1093/bioinformatics/bts697.
50
51
52 512 12. Stewart C, Kural D, Stromberg MP, Walker JA, Konkel MK, Stutz AM, et al. A comprehensive
53 map of mobile element insertion polymorphisms in humans. *PLoS Genet*. 2011;7 8:e1002236.
54
55 513
56
57 514 doi:10.1371/journal.pgen.1002236.
58
59
60
61
62
63
64
65

- 1 515 13. Ewing AD and Kazazian HH, Jr. Whole-genome resequencing allows detection of many rare
2
3 516 LINE-1 insertion alleles in humans. *Genome research.* 2011;21 6:985-90.
4
5 517 doi:10.1101/gr.114777.110.
6
7 518 14. Sudmant PH, Rausch T, Gardner EJ, Handsaker RE, Abyzov A, Huddleston J, et al. An
8 integrated map of structural variation in 2,504 human genomes. *Nature.* 2015;526 7571:75-81.
9
10 519
11
12 520 doi:10.1038/nature15394.
13
14
15 521 15. Xing J, Witherspoon DJ and Jorde LB. Mobile element biology: new possibilities with
16 high-throughput sequencing. *Trends in genetics : TIG.* 2013;29 5:280-9.
17
18 522
19
20 523 doi:10.1016/j.tig.2012.12.002.
21
22
23 524 16. Lan, T; Lin, H; Asker Melchior Tellier, L, C; Zhu, W; Yang, M; Liu, X; Wang, J; Wang, J; Yang,
24
25 H; Xu, X; Guo, X (2017): Deep whole-genome sequencing of 90 Han Chinese genomes.
26
27 525
28
29 526 GigaScience. In Press.
30
31
32 527 17. Wang J, Wang W, Li R, Li Y, Tian G, Goodman L, et al. The diploid genome sequence of an
33 Asian individual. *Nature.* 2008;456 7218:60-5. doi:10.1038/nature07484.
34
35
36 528
37
38 529 18. Li H and Durbin R. Fast and accurate short read alignment with Burrows-Wheeler transform.
39
40 530 *Bioinformatics.* 2009;25 14:1754-60. doi:10.1093/bioinformatics/btp324.
41
42
43 531 19. McKenna N, Hanna M, Banks E, Sivachenko A, Cibulskis K, Kernytsky A, et al. The Genome
44 Analysis Toolkit: a MapReduce framework for analyzing next-generation DNA sequencing data.
45
46
47 532
48
49 533 Genome research. 2010;20 9:1297-303. doi:10.1101/gr.107524.110.
50
51
52 534 20. Jurka J, Kapitonov VV, Pavlicek A, Klonowski P, Kohany O and Walichiewicz J. Repbase
53
54
55 535 Update, a database of eukaryotic repetitive elements. *Cytogenet Genome Res.* 2005;110
56
57
58 536 1-4:462-7. doi:10.1159/000084979.

- 1 537 21. Wang J, Song L, Grover D, Azrak S, Batzer MA and P L. dbRIP: a highly integrated database of
2 538 retrotransposon insertion polymorphisms in humans. *Hum Mutat.* 2006;27 4:323-9.
3
4 539 22. Hormozdiari F, Hajirasouliha I, Dao P, Hach F, Yorukoglu D, Alkan C, et al. Next-generation
5 VariationHunter: combinatorial algorithms for transposon insertion discovery. *Bioinformatics.*
6 540 2010;26 12:i350-7. doi:10.1093/bioinformatics/btq216.
7
8 541
9
10 542 23. Mount DW. Using the Basic Local Alignment Search Tool (BLAST). *CSH Protoc.*
11
12 543 2007;2007:pdb top17. doi:10.1101/pdb.top17.
13
14 544 24. Baillie JK, Barnett MW, Upton KR, Gerhardt DJ, Richmond TA, De Sario F, et al. Somatic
15 retrotransposition alters the genetic landscape of the human brain. *Nature.* 2011;479 7374:534-7.
16
17 545
18
19 546 doi:10.1038/nature10531.
20
21
22 547 25. Boissinot S, Chevret P and AV F. L1 (LINE-1) retrotransposon evolution and amplification in
23 recent human history. *Mol Biol Evol.* 2000;17 6:915-28.
24
25
26 548
27
28 549 26. Dombroski BA, Mathias SL, Nanthakumar E, Scott AF and Jr KH. Isolation of an active human
29 transposable element. *Science.* 1991;254 5039:1805-8.
30
31
32 550
33
34 551 27. Ovchinnikov I, Rubin A and GD S. Tracing the LINEs of human evolution. *Proceedings of the*
35
36 552 *National Academy of Sciences of the United States of America.* 2002;99 16:10522-7.
37
38
39 553 28. Ovchinnikov I, Troxel AB and GD S. Genomic characterization of recent human LINE-1
40 insertions: evidence supporting random insertion. *Genome research.* 2001;11 12:2050-8.
41
42
43 554
44
45 555 29. Huang X and Madan A. CAP3: A DNA sequence assembly program. *Genome research.* 1999;9
46
47 556 9:868-77.
48
49
50 557 30. Altschul SF, Gish W, Miller W, Myers EW and Lipman DJ. Basic local alignment search tool.
51
52
53 558 *Journal of molecular biology.* 1990;215 3:403-10.
54
55
56
57
58
59
60
61
62
63
64
65

- 1 559 31. Hu X, Yuan J, Shi Y, Lu J, Liu B, Li Z, et al. pIRS: Profile-based Illumina pair-end reads
2
3 560 simulator. Bioinformatics. 2012;28 11:1533-5.
4
5 561 32. Tarailo-Graovac M and Chen N. Using RepeatMasker to identify repetitive elements in
6 genomic sequences. Curr Protoc Bioinformatics. 2009;Chapter 4:Unit 4 10.
7
8 562 doi:10.1002/0471250953.bi0410s25.
9
10 563
11
12 564 33. Hormozdiari F, Alkan C, Ventura M, Hajirasouliha I, Malig M, Hach F, et al. Alu repeat
13 discovery and characterization within human genomes. Genome research. 2011;21 6:840-9.
14
15 565 doi:10.1101/gr.115956.110.
16
17 566
18
19 567 34. Batzer MA and Deininger PL. Alu repeats and human genomic diversity. Nature reviews
20 Genetics. 2002;3 5:370-9. doi:10.1038/nrg798.
21
22
23 568
24
25 569 35. Burns KH and Boeke JD. Human transposon tectonics. Cell. 2012;149 4:740-52.
26
27
28 570 doi:10.1016/j.cell.2012.04.019.
29
30
31 571 36. Wang J, Song L, Grover D, Azrak S, Batzer MA and Liang P. dbRIP: a highly integrated
32 database of retrotransposon insertion polymorphisms in humans. Hum Mutat. 2006;27 4:323-9.
33
34
35 572
36
37 573 doi:10.1002/humu.20307.
38
39
40 574 37. Tajima F. Statistical method for testing the neutral mutation hypothesis by DNA polymorphism.
41
42
43 575 Genetics. 1989;123 3:585-95.
44
45
46 576 38. Boyko AR, Williamson SH, Indap AR, Degenhardt JD, Hernandez RD, Lohmueller KE, et al.
47
48
49 577 Assessing the evolutionary impact of amino acid mutations in the human genome. PLoS Genet.
50
51
52 578 2008;4 5:e1000083. doi:10.1371/journal.pgen.1000083.
53
54
55 579 39. Rigat B, Hubert C, Alhenc-Gelas F, Cambien F, Corvol P and F S. An insertion/deletion
56 polymorphism in the angiotensin I-converting enzyme gene accounting for half the variance of
57
58 580
59
60
61
62
63
64
65

- 1 581 serum enzyme levels. J Clin Invest. 1990;86 4:1343-6.
- 2
- 3 582 40. Jeng JR, Harn HJ, Jeng CY, Yueh KC and SM S. Angiotensin I converting enzyme gene
- 4
- 5 583 polymorphism in Chinese patients with hypertension. Am J Hypertens. 1997;10 5Pt1:558-61.
- 6
- 7
- 8 584 41. Zee RY, Lou YK, Griffiths LR and BJ M. Association of a polymorphism of the angiotensin
- 9
- 10
- 11 585 I-converting enzyme gene with essential hypertension. Biochem Biophys Res Commun.
- 12
- 13 586 1992;184 1:9-15.
- 14
- 15
- 16
- 17 587 42. Asamoah A, Yanamandra K, Thurmon TF, Richter R, Green R, Lakin T, et al. A deletion in the
- 18
- 19 588 angiotensin converting enzyme (ACE) gene is common among African Americans with
- 20
- 21 589 essential hypertension. Clin Chim Acta. 1996;254 1:41-6.
- 22
- 23
- 24
- 25 590 43. Duru K, Farrow S, Wang JM, Lockette W and T K. Frequency of a deletion polymorphism in
- 26
- 27 591 the gene for angiotensin converting enzyme is increased in African-Americans with
- 28
- 29 592 hypertension. Am J Hypertens. 1994;7 8:759-62.
- 30
- 31
- 32
- 33 593 44. Anand SS, Yusuf S, Vuksan V, Devanesen S, Teo KK, Montague PA, et al. Differences in risk
- 34
- 35 594 factors, atherosclerosis, and cardiovascular disease between ethnic groups in Canada: the Study
- 36
- 37 595 of Health Assessment and Risk in Ethnic groups (SHARE). Lancet. 2000;356 9226:279-84.
- 38
- 39
- 40
- 41 596 45. Batzer MA, Stoneking M, Alegria-Hartman M, Bazan H, Kass DH, Shaikh TH, et al. African
- 42
- 43 597 origin of human-specific polymorphic Alu insertions. Proceedings of the National Academy of
- 44
- 45 598 Sciences of the United States of America. 1994;91 25:12288-92.
- 46
- 47
- 48
- 49 599 46. Qichao Yu. (2016, September 1). Specific Insertions Detector. Zenodo.
- 50
- 51 600 <http://doi.org/10.5281/zenodo.212115>
- 52
- 53
- 54
- 55 601 47. Zong C, Lu S, Chapman AR and Xie XS. Genome-wide detection of single-nucleotide and
- 56
- 57 602 copy-number variations of a single human cell. Science. 2012;338 6114:1622-6.
- 58
- 59
- 60
- 61
- 62
- 63
- 64
- 65

1 603 doi:10.1126/science.1229164.
2
3 604 48. Lan, T; Lin, H; Asker Melchior Tellier, L, C; Zhu, W; Yang, M; Liu, X; Wang, J; Wang, J; Yang,
4
5 605 H; Xu, X; Guo, X (2017): Supporting data for "Deep whole-genome sequencing of 90 Han
6
7 606 Chinese genomes" GigaScience Database. <http://dx.doi.org/10.5524/100302>
8
9 607 49. Yu, Q; Zhang, W; Zeng, Y; Zhang, X; Wang, Y; Wang, Y; Xu, L; Huang, X; Li, N; Zhou, X; Lu,
10
11 608 J; Guo, X; Li, G; Hou, Y; Liu, S; Li, B (2017): Supporting data for "Population-wide Sampling
12
13 609 of Retrotransposon Insertion Polymorphisms Using Deep Sequencing and Efficient Detection"
14
15 610 GigaScience Database. <http://dx.doi.org/10.5524/100318>
16
17 611 50 Haoxiang Lin: SNP INDEL calling. [protocols.io dx.doi.org/10.17504/protocols.io.grkbv4w](http://dx.doi.org/10.17504/protocols.io.grkbv4w)
18
19 612 51. GigaScience Database: Simulating reads for detection of transportable element insertions.
20
21 613 [protocols.io. 2017. dx.doi.org/10.17504/protocols.io.imrcc56](http://dx.doi.org/10.17504/protocols.io.imrcc56)
22
23 614
24
25 615
26
27
28 616 **Figure legends**
29
30
31
32
33
34
35
36
37
38
39 617 **Fig. 1** The principle of retrotransposon insertion detection. **(a)** Schematic diagram of using SID
40
41 618 for RIP detection in the genome. TSD: target site duplication. SID: Specific Insertions Detector.
42
43
44 619 **(b)** An example of reads mapping for predicted homozygous insertions. **(c)** An example of
45
46 620 reads mapping for predicted heterozygous insertions. In **(b)** and **(c)**, the red bases indicate the
47
48 621 mismatches, and the sequences with an orange background represent the clipped part of the
49
50 622 reads. The clipped reads are derived from one allele with inserted retrotransposons, and the
51
52
53 623 normal reads are derived from the other allele with the same reference. The three reads with
54
55
56 624 asterisks indicate no clipped part but the presence of terminal mismatches, which can also

1 625 support the breakpoint and exhibit consistency with the clipped reads.
2
3

4 626 **Fig. 2** Assessing the SID results. (a) Detecting accuracy and sensitivity estimation along
5 cumulating sequencing depth of simulated data. (b) RIP genotyping of YH_CL. PCR validation
6
7 627 results are marked. HEE: estimated heterozygous site. HOE: estimated homozygous site.
8
9 628 HEV: validated heterozygous site. HOV: validated homozygous site. The dash line indicates
10 the estimated boundary between heterozygous and homozygous sites. Note that some of the
11 validated RIPS are present in the same locus in the plot figure.
12
13

14 629 **Fig. 3** Comprehensive landscape of non-reference RIPS of YH90. (a) Proportions of novel
15 insertions identified for each type of retrotransposon. (b) Comparison of YH90 non-reference
16 RIPS results with dbRIP. Adjacent 100-bp regions of RIPS were taken into consideration. (c) TE
17 distribution of each YH90 sample. (d) Box plots of non-reference RIP distribution among
18 autosomes. (e) TE frequency distribution among YH90 samples. Rings from outer to inner
19 indicate Alu insertion frequency, L1 insertion frequency, SVA insertion frequency, LTR
20 insertion frequency and cytoband structure. The inside frequency of the rings indicates the
21 insertion frequency for the Northern Chinese group, and the outside frequency represents that
22 of the Southern Chinese group. (f) RIP distribution in different functional regions of the
23 genome.
24
25

26 642 **Fig. 4** Population genetics analysis based on YH90. (a) A two-epoch population with a recent
27 contraction; a three-epoch bottleneck-shaped history, which contained a reduction of the
28 effective population size in the past followed by a recent phase of size recovery. Details of the
29 parameters for all models are provided in Additional file 2: Table S12. (b) The observed SNP
30
31

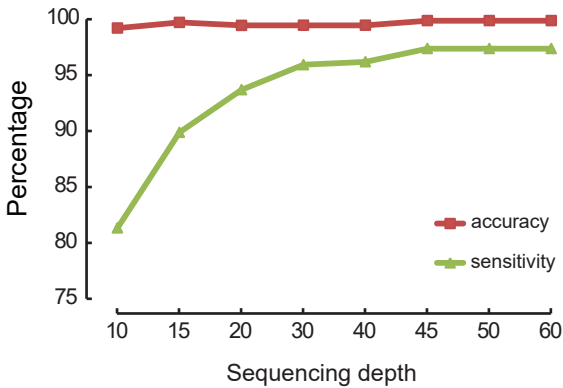
1 frequency spectra and expected neutral SNP frequency spectra under different demographic
2
3 models. (c) Observed and expected RIP site frequency spectra before demographic correction
4
5 of each subfamily. (d) Assessing the evolutionary impact of RIPs in the human genome. The
6
7 allele frequency distribution of RIPs was compared among observed, neutral models and
8
9 negative models after demographic correction.
10
11
12

13
14
15 **Fig. 5** Phylogenetic analysis using RIPs and SNPs. (a) The detected RIPs were used for PCA.
16
17 Each dot represents a sample from YH90 and is plotted as scatterplot using PC1 and PC2.
18
19 Red indicates samples from individuals from northern China, and blue indicates individuals
20
21 from southern China. (b) The detected SNPs were used for PCA. The plot layout and legend
22
23 are the same as those presented in (a). (c) Phylogenetic tree constructed using the detected
24
25 RIPs. HG19 (green) is used as a control. Red indicates samples from individuals from northern
26
27 China, and blue indicates samples from individuals from southern China. (d) Phylogenetic tree
28
29 constructed using the detected SNPs. HG19 (green) is used as a control. Plot layout and
30
31 legend are same as that presented in (c).
32
33
34
35
36
37
38
39
40
41
42
43
44
45
46
47
48
49
50
51
52
53
54
55
56
57
58
59
60
61
62
63
64
65

Figure 2

[Click here to download Figure Fig. 2.pdf](#) 

A



B

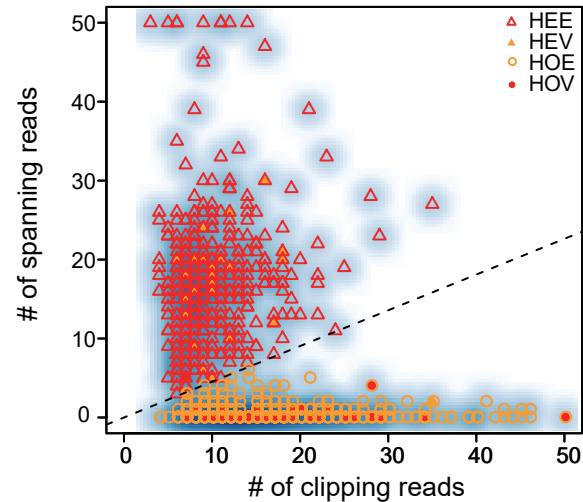


Figure 3

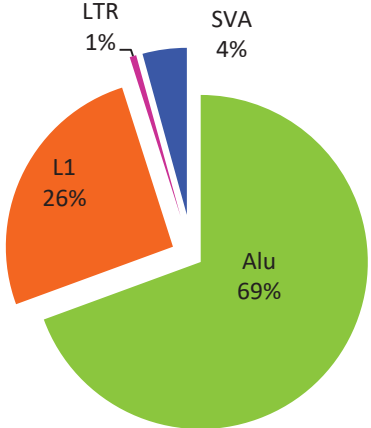
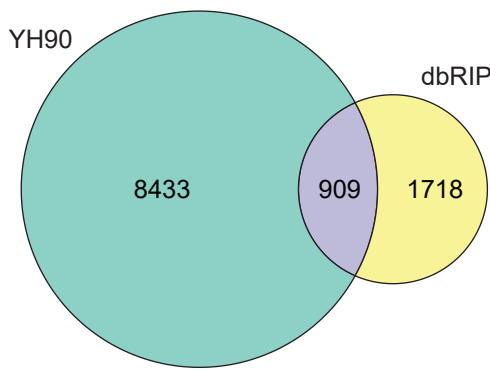
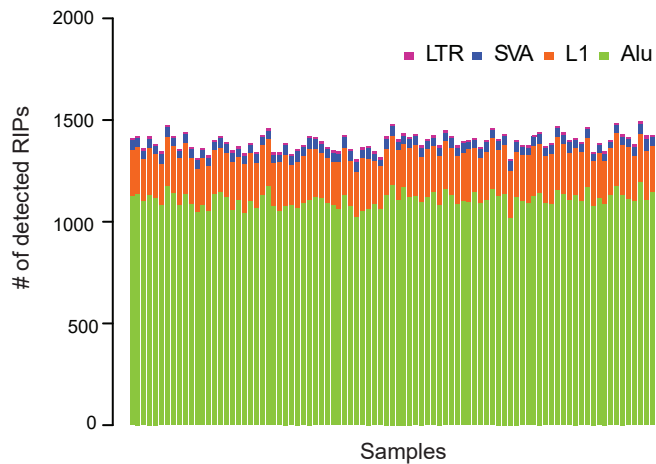
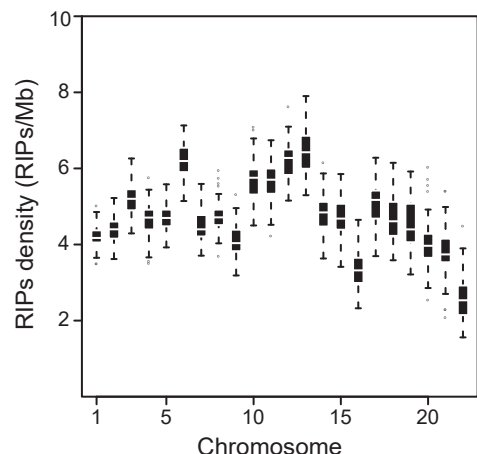
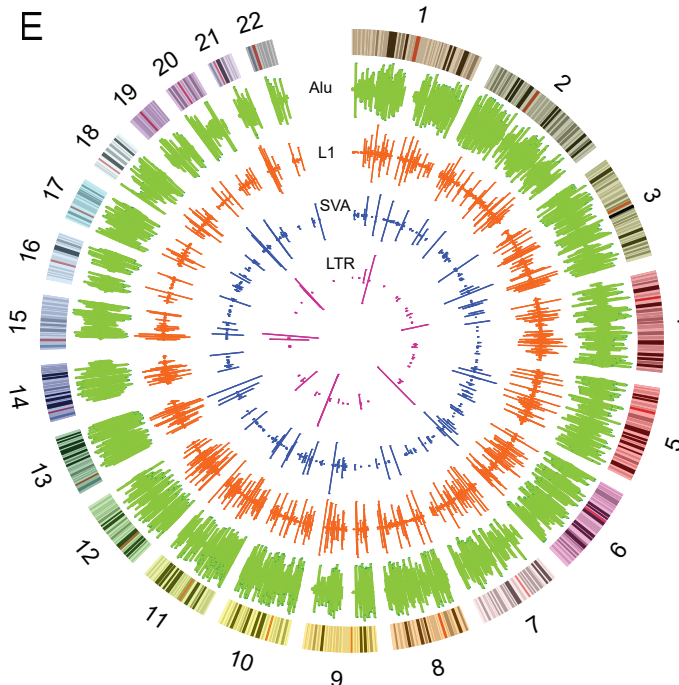
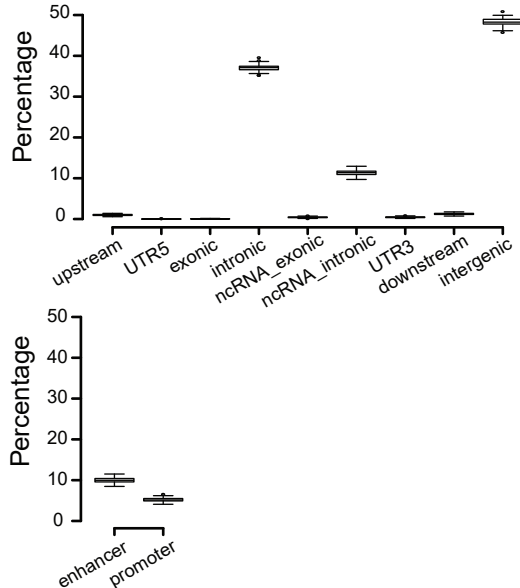
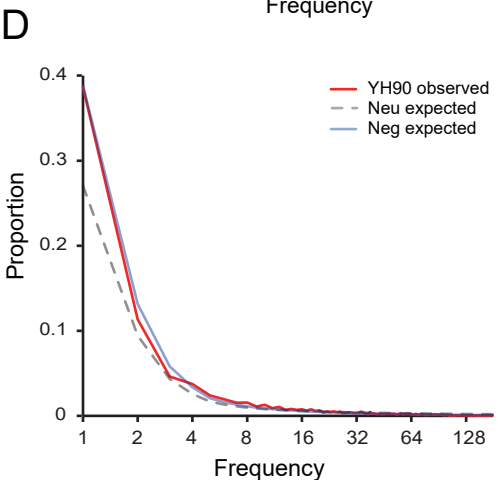
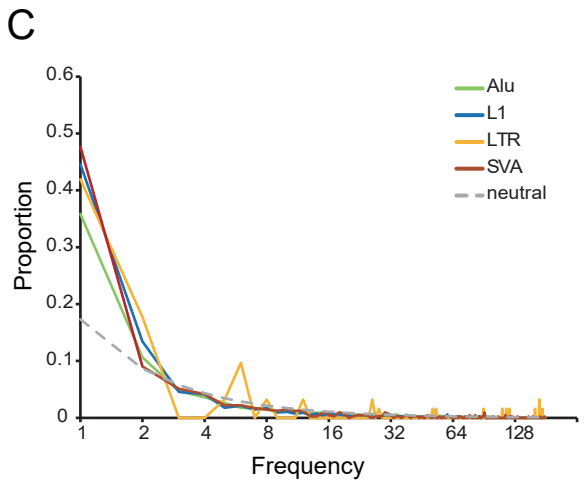
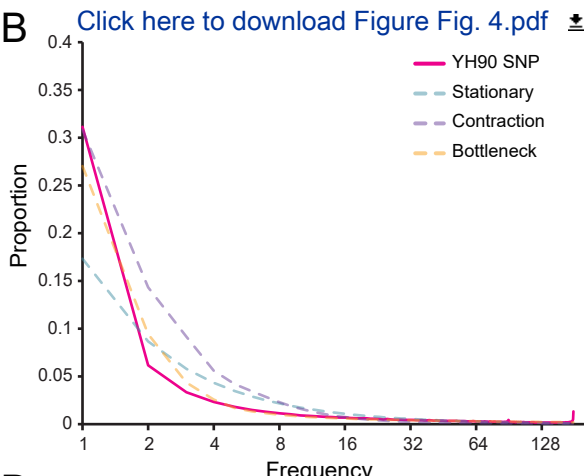
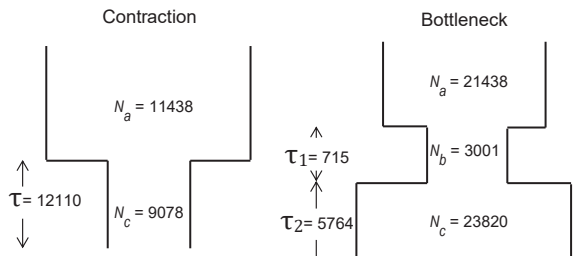
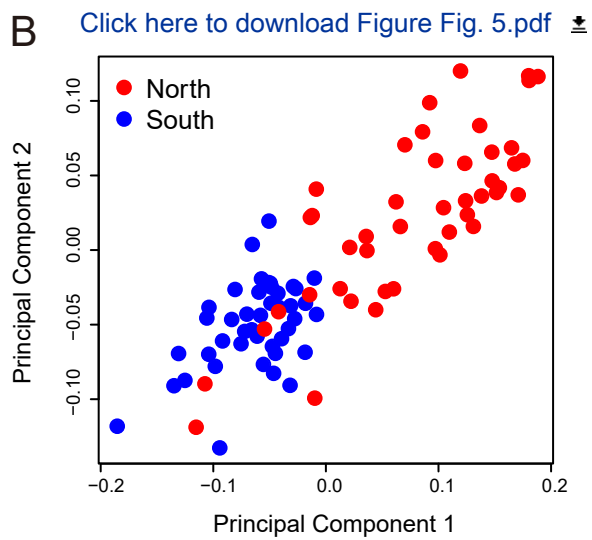
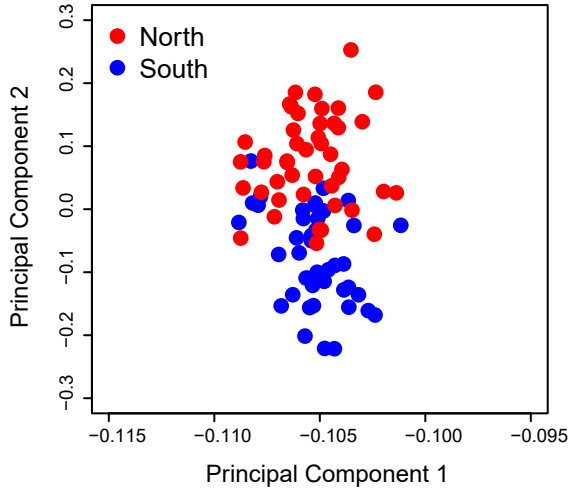
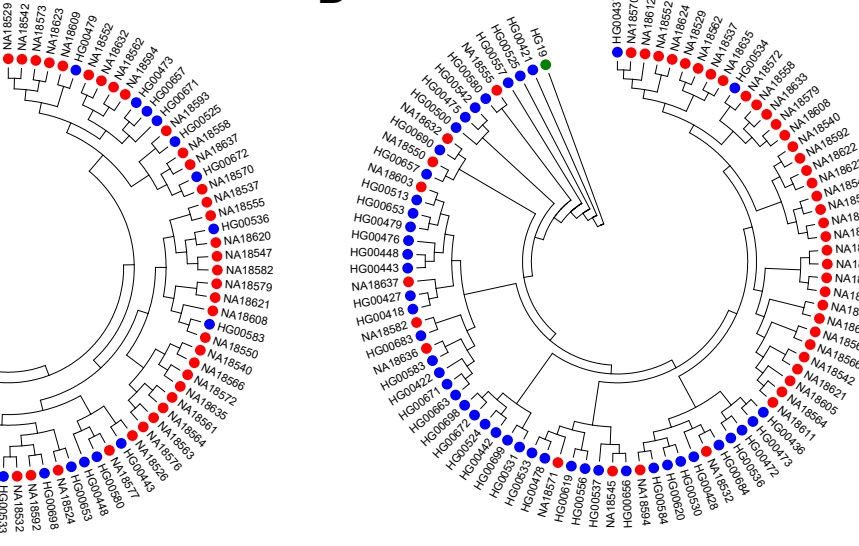
[Click here to download Figure Fig. 3.pdf](#)
A**B****C****D****E****F**

Figure 4

A Figure 5 [Click here to download Figure Fig. 5.pdf](#)



C





Click here to access/download
Supplementary Material
Additional file 1.xlsx



Click here to access/download
Supplementary Material
Additional file 2.pdf